Proceedings of IMECE2007
2007 ASME International Mechanical Engineering Congress and Exposition
November 11-15, 2007, Seattle, Washington, USA

IMECE2007-42347

DESIGN OF CONTROLLERS FOR A MULTI-DEGREE-OF-FREEDOM SPHERICAL WHEEL MOTOR

Hungsun Son
Ph. D. Candidate, Woodruff School of Mechanical Engineering
Georgia Institute of Technology
Atlanta, GA 30332-0405

Kok-Meng Lee
Professor, Woodruff School of Mechanical Engineering
Georgia Institute of Technology
Atlanta, GA 30332-0405

ABSTRACT

This paper presents the control system design for a particular form of variable-reluctance spherical motors, referred to here as a spherical wheel motor (SWM). Unlike most of the existing spherical motors where focuses have been on the control of the three-DOF angular displacement, the SWM offers a means to control the orientation of a continuously rotating shaft. Specifically, we demonstrate an effective method to decouple the open-loop (OL) control of the spin rate from that of the inclination, leading to a practical OL system combining a switching (spin-rate) controller and a model-based inclination controller. The OL system presented here provides the fundamental control structure for the SWM. To account for un-modeled external torques, we extend the design to allow feedback with a PD controller and a high-gain observer. The effectiveness of the controllers has been investigated by comparing their performance numerically under the influence of an unknown external torque.

INTRODUCTION

Growing demands for miniature devices in modern industries involving natural products and/or bio-tissues have motivated the development of novel actuators for high-speed spindles and high-accuracy stages capable of precision orientation/torque control of the machine tool or work piece [1]. Existing multi-DOF manipulators [2-3] generally use a combination of single-axis actuators to control their orientation. They also require an external force/torque sensor for applications (such as bio-medical surgery or cutting of highly deformable materials). Driven by stringent accuracy and tolerance requirements, various forms of micro-motion parallel mechanisms with three or more single-axis actuators were proposed. These multi-DOF mechanisms, however, are generally bulky, and lack of dexterity in negotiating the orientation of the cutter or work-piece. Ball-joint-like actuators (capable of three-DOF orientation in a single joint with built-in force/torque estimation) offer an attractive solution to eliminate motion singularities.

Most existing spherical motors have been developed on the operational principles similar to their single-axis counterparts; for example, DC, switched reluctance (SR), or PM stepper motors. However, closed-loop control systems for multi-DOF spherical motors are much more difficult to design due to their nonlinear rotor dynamics, complex magnetic fields, and challenging measurement problems. Nevertheless, controller design techniques for single-axis actuators can be extended to multi-DOF spherical motors, and are further explored here.

Recently, nonlinear control techniques for single-axis motors (such as nonlinear observer, feedback linearization, adaptive and robust control, etc.) have been studied by numerous researchers. By expanding the system and measurement functions about the current estimate state, Ueda et al. [4] applied a new nonlinear (or extended linear) observer that estimates the transient state of the power system to a smooth-rotor synchronous generator. Lawrence et al. [5] derived an identity state observer for a PM synchronous motor by reconstructing the electrical and mechanical states of the motor from the current and voltage measurements; their nonlinear observer (described in the rotor coordinate frame) estimates the stator currents, and the rotor velocity and position. High-gain observer techniques have recently been demonstrated to play an important role in the design of output feedback control of nonlinear systems. Dabroom et al. [6] proposed the digital control of nonlinear systems using high-gain observers. They experimentally validated the closed-loop analysis and showed that the sampled-data controller recovers the performance of the continuous time controller as the sampling frequency and observer gain become sufficiently large. Zhu et al. [7] proposed a linearization-based controller with a nonlinear state observer which estimates the rotor position and speed, and demonstrated the stability of the closed-loop system, including the observer through the Lyapunov stability theory.

The remainder of this paper offers the following:

1. We present the mechanical structure of a multi-DOF SWM designed for manipulating the orientation of a continuously rotating shaft. Based on this design, we derive the torque

model in closed form, which is essential for dynamics modeling and controller design of the motor.

2. We develop three controllers for the SWM and present their characteristics; namely, open-loop (OL), PD, and PD with a high-gain observer. The OL controller consists of two parts. The 1st part is a switching controller based on the principle of a VR stepper [1] [8] for regulating the spin rate, while the 2nd part is based on the inverse torque model for manipulating the inclination. The OL controller provides the fundamental design structure for the SWM and thus severs as a basis for the other two feedback controller designs.
3. We illustrate the effectiveness of the controllers by simulation and compare their performance under the influence of an unknown external torque.

MECHANICAL STRUCTURE AND DYNAMIC MODEL

Figure 1(a) shows the CAD model of a SWM consisting of 16 rotor PM's and 20 stator EM's equally spaced on four circular planes. As shown in Fig. 1(b), the PM's and EM's are grouped in pairs and every two pole-pairs form a plane, and their magnetization axes pass radially through the center. The SWM structure has a well-balanced symmetry electro mechanically. The magnetization axes of the m_r rotor PM pole pairs and m_s stator EM pole-pairs are given by (1) and (2) respectively in their own body coordinate frames:

$$\mathbf{x}_{\mathbf{m}i} = (-1)^{i-1}\begin{bmatrix}\cos\phi_r\cos\delta_{ri} & \cos\phi_r\sin\delta_{ri} & \sin\phi_r\end{bmatrix}^{\mathrm{T}} \quad (1)$$

where $i = 1, 2 \ldots m_r$; $\delta_{ri} = (i-1)\delta_r$; and $\delta_r = 2\pi / m_r$.

$$\mathbf{X}_{\mathbf{s}\,j} = \begin{bmatrix}\cos\phi_s\cos\delta_{sj} & \cos\phi_s\sin\delta_{sj} & \sin\phi_s\end{bmatrix}^{\mathrm{T}} \quad (2)$$

where $j = 1, 2 \ldots m_s$; $\delta_{sj} = (j-1)\delta_s$; and $\delta_s = 2\pi / m_s$. In (1) and (2), ϕ_r and ϕ_s are the angles between the magnetization axes and the XY plane defined in Fig. 1(b). Unlike m_s which may be odd or even, m_r is always an even number.

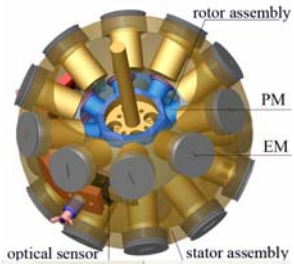

(a) CAD model [8]

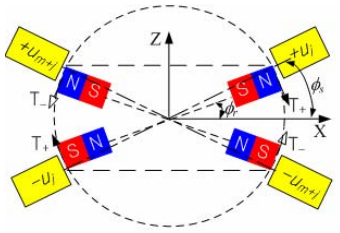

(b) Stator and rotor pole-pairS

Fig. 1 Schematics illustrating the mechanical structure of a SWM

Torque Model

Magnetic forces involved in the SWM can be calculated using the *Lorenz* force equation:

$$\mathbf{F} = -\oint \mathbf{B} \times Id\boldsymbol{\ell} \qquad \text{where} \qquad I = -\iint \mathbf{J} \bullet d\mathbf{S} \quad (3a,b)$$

where **B** is the magnetic field; I is current through the conductor; and $\boldsymbol{\ell}$ is the normalized vector of the current direction**.** In (3b), the current density vector **J** is directly used in the calculation and thus, it is not necessary to compute the magnetic flux generated by the current loop. Thus, the Lorenz force calculation involves only the **B**-fields of the permanent magnets. The magnetic field **B** of the rotor PM's can be computed by the DMP method [9-10], which gives the solution in closed form. However, the PM's rotates with respects to the stator EM's. To compute the force acting on the current-carrying j^{th} EM, the total magnetic field **B** is expressed in the j^{th} EM coordinates $\mathbf{x}_{cj}$. Figure 2 shows the XYZ Euler angles (α, β, γ), which has no singularity in the domain of interest, for the coordinate transformation from the rotor $\mathbf{x}_{\mathbf{r}}$ to the stator $\mathbf{x}_{\mathbf{s}}$. In the local coordinate system of the j^{th} EM, the position of the i^{th} PM is given by (4):

$$\mathbf{x}_{cj} = \begin{bmatrix}\mathbf{L}_{cj\mathbf{s}}\end{bmatrix}\begin{bmatrix}\mathbf{L}_{\mathbf{sr}}\end{bmatrix}\mathbf{x}_{mi} \quad (4)$$

where $\begin{bmatrix}\mathbf{L}_{\mathbf{sr}}\end{bmatrix} = \begin{pmatrix} C_\gamma C_\beta & C_\gamma S_\alpha S_\beta & -C_\gamma C_\alpha S_\beta + S_\gamma S_\alpha \\ -S_\gamma C_\beta & C_\alpha C_\gamma - S_\gamma S_\alpha S_\beta & S_\gamma C_\alpha S_\beta + C_\gamma S_\alpha \\ S_\beta & -S_\alpha C_\beta & C_\alpha C_\beta \end{pmatrix}$;

$\begin{bmatrix}\mathbf{L}_{\mathbf{cjs}}\end{bmatrix} = \begin{pmatrix} C_{\phi_s} & -S_{\phi_s} & 0 \\ S_{\theta_{sj}} S_{\phi_s} & S_{\theta_{sj}} C_{\phi_s} & C_{\theta_c} \\ -C_{\theta_{sj}} S_{\phi_s} & -C_{\theta_{sj}} C_{\phi_s} & S_{\theta_c} \end{pmatrix}$; C and S represent cosine and sine respectively; and the subscripts of C and S denote their respective angles.

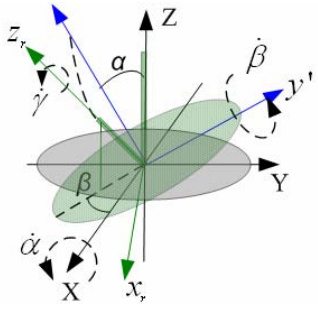

Fig. 2 XYZ Coordinate transformation

Once the force acting on the j^{th} EM is computed, the resultant torque for all EM's can be computed from (5):

$$\mathbf{T}_{\text{total}} = \begin{bmatrix}T_X & T_Y & T_Z\end{bmatrix}^{\mathrm{T}} = \begin{bmatrix}\tilde{\mathbf{T}}_1 & \tilde{\mathbf{T}}_2 & \ldots & \tilde{\mathbf{T}}_{\mathbf{m_s}}\end{bmatrix}\mathbf{u} \quad (5)$$

where $\tilde{\mathbf{T}}_{\mathbf{j}} \left(\in \mathbb{R}^{3\times 1}\right) = \mathbf{L}_{\mathbf{cjs}}^{\mathrm{T}} \left(\oint_{EM} \left[\sum_i m_i \beta_i(\alpha,\beta,\gamma) \right] dSdL \right)$; and

$\mathbf{u} = \begin{bmatrix} J_1 & J_2 & \ldots & J_{m_s} \end{bmatrix}^{\mathrm{T}}$

The torque vector (5) is orientation dependent and must be evaluated numerically from the volume integral in real time. To reduce the computation to a tractable form, we take advantages that the torque is linearly proportional to the current and hence apply the principle of superposition [8][9] to compute the total magnetic torque acting on the rotor:

$$\mathbf{T}_{total} \approx \begin{bmatrix}\hat{\mathbf{K}}_1 & \cdots & \hat{\mathbf{K}}_{\mathbf{j}} & \cdots & \hat{\mathbf{K}}_{\mathbf{m_s}}\end{bmatrix}\mathbf{u} \quad (6a)$$

$$\hat{\mathbf{K}}_{\mathbf{j}} = \begin{cases} -\sum_{k=1}^{m_r} \left\{ \hat{f}(\varphi)\Big|_{\varphi=\varphi_{jk}} \dfrac{\mathbf{s}_j \times \mathbf{r}_k}{|\mathbf{s}_j \times \mathbf{r}_k|} \right\} & \text{if } \mathbf{s}_j \times \mathbf{r}_k \neq 0 \\ 0 & \text{if } \mathbf{s}_j \times \mathbf{r}_k = 0 \end{cases} \quad (6b)$$

where $\hat{f}(\varphi)$ curve-fits the torque between a PM pole-pair and an EM pole-pair in terms of the separation angle φ given by (7):

$$\varphi_{jk} = \cos^{-1}\left(\mathbf{s}_j \bullet \mathbf{r}_k\right) / \left(\left|\mathbf{s}_j\right|\left|\mathbf{r}_k\right|\right). \quad (7)$$

Equation of Motion

The equation of motion can be derived using the Lagrangian formulation in terms of the XYZ Euler angles (α, β, γ), which has the following form:

$$[\mathbf{M}]\dot{q}_2 + \mathbf{C}(q_1, q_2) + \mathbf{C}_f = \mathbf{Q} + \mathbf{T}_{\mathbf{ext}} \quad (8)$$

where $q_1 = [\alpha \ \beta \ \gamma]^{\mathrm{T}}$; $q_2 = \dot{q}_1$; $\mathbf{T}_{\mathbf{ext}}$ is the disturbance torque; $\mathbf{C}_f$ is the frictional torque of mechanical bearing; and where

$$\mathbf{M} = \begin{bmatrix} I_t C_\beta^2 + I_a S_\beta^2 & 0 & -I_t S_\beta \\ 0 & I_t & 0 \\ -I_t S_\beta & 0 & I_a \end{bmatrix} \quad (8a)$$

$$C(\dot{q}, q) = \begin{bmatrix} 2(I_a - I_t) S_\beta C_\beta \dot{\alpha}\dot{\beta} - I_a C_\beta \dot{\beta}\dot{\gamma} \\ (I_t - I_a) S_\beta C_\beta \dot{\alpha}^2 + I_a C_\beta \dot{\alpha}\dot{\gamma} \\ -I_a C_\beta \dot{\alpha}\dot{\beta} \end{bmatrix} \quad (8b)$$

and $$\mathbf{Q} = \begin{bmatrix} -S_\beta C_\gamma & S_\beta S_\gamma & C_\beta \\ S_\gamma & C_\gamma & 0 \\ 0 & 0 & 1 \end{bmatrix} \begin{Bmatrix} T_X \\ T_Y \\ T_Z \end{Bmatrix} \quad (8c)$$

In (8a,b), $I_a = I_{zz}$; $I_t = I_{xx} = I_{yy}$; and the mass center of the rotor is assumed to coincide with the center of rotation. In (8c), **Q** is in *xyz* rotor coordinates and represents the contributions of the applied (magnetic) torque to the generalized moments. Since the inertia matrix [M] is positive-definite in the range of inclination motion (-20°≤ α, β≤ 20°), the nonlinear dynamics (8) can be expressed in the standard state forms as

$$\dot{q} = \begin{bmatrix} q_1 \\ q_2 \end{bmatrix} = \begin{bmatrix} 0_{3\times3} & I_{3\times3} \\ f(q) \end{bmatrix} + \begin{bmatrix} 0_{3\times3} \\ I_{3\times3} \end{bmatrix} \mathbf{Q} \quad (9)$$

where $f(q) = [\mathbf{M}]^{-1}\mathbf{C}(q) \in R^{3\times1}$ is given by

$$f(q) = \frac{1}{I_t}\begin{bmatrix} q_5 \sec q_2 \left(I_a q_6 + (2I_t - 3I_a) q_4 S_{q_2}\right) \\ q_4 C_{q_2}\left(-I_a q_6 + (I_t - I_a) q_4 S_{q_2}\right) \\ q_5\left\{-I_t q_4 C_{q_2} + \left[I_a q_6 + (2I_t - 3I_a) q_4 S_{q_2}\right]\tan q_2\right\} \end{bmatrix} \quad (9a)$$

which is linearized around the desired state for observer design:

$$[\mathbf{A}] = \left(\frac{\partial f_j}{\partial q_i}\right)\Big|_{q=q_d} = \frac{1}{I_t}\begin{bmatrix} [\mathbf{A}_1] & [\mathbf{A}_2] \\ [\mathbf{A}_3] & [\mathbf{A}_4] \end{bmatrix}_{q=q_d} \quad (9b)$$

where $[\mathbf{A}_1] = [0_{3\times3}]$; $[\mathbf{A}_2] = I_t[\mathbf{I}_{3\times3}]$; **I** is the identity matrix;

$$[\mathbf{A}_3] = \begin{bmatrix} 0 & A_{42} & 0 \\ 0 & A_{52} & 0 \\ 0 & A_{62} & 0 \end{bmatrix}_{q=q_d}; \quad [\mathbf{A}_4] = \begin{bmatrix} A_{44} & A_{45} & A_{46} \\ A_{54} & 0 & A_{56} \\ A_{64} & A_{65} & A_{66} \end{bmatrix}_{q=q_d};$$

$A_{42} = q_5\left(2I_t q_4 - 3I_a q_4 + 3I_a q_6 \sin q_2\right)\sec^2 q_2$;

$A_{52} = q_4\left[(I_1 - I_3) q_4 \cos 2q_2 + I_3 q_6 \sin q_2\right]$;

$A_{62} = q_5\left[I_a q_6 \sec^2 q_2 + 3(I_t - I_a) q_4 \sin 2q_2 + (2I_t - 3I_a) q_4 \sec q_2 \tan q_2\right]$;

$A_{44} = (2I_t - 3I_a) q_5 \tan q_2$; $A_{54} = \left[2(I_1 - I_3) q_4 \sin q_2 - I_3 q_6\right]\cos q_2$;

$A_{64} = q_5\left[(2I_t - 3I_a)\sin q_2 \tan q_2 - I_t \cos q_2\right]$;

$A_{45} = \left[I_a q_6 + (2I_t - 3I_a) q_4 \sin q_2\right]\sec q_2$;

$A_{65} = \left[I_a q_6 + (2I_t - 3I_a) q_4 \sin q_2\right]\tan q_2 - I_t q_4 \cos q_2$; and

$A_{46} = I_a q_5 \sec q_2$; $A_{56} = -I_3 q_4 \cos 2q_2$; and $A_{66} = I_a q_5 \tan q_2$

CONTROLLER DESIGN OF SWM

We illustrate three SWM controllers; OL, PD, and a high-gain observer. The OL controller provides the fundamental design structure for the SWM and thus severs as a basis for the other two feedback controller designs.

A. Open-loop (OL) Controller

A model-based OL controller (that is designed to perform orientation control of a continuously spinning rotor as shown in Fig. 3) consists of two parts; one for the (α, β) inclination, and the other for the spin rate $\dot{\gamma}$ (or switching control). The amplitude-modulated current inputs of the SWM have the following form:

$$u_{sj} = \mathrm{sat}\left[u_{\gamma j}\left(1 + u_{\alpha\beta j}\right)\right] \quad \text{where } j=1,2,\ldots m_s \quad (10)$$

where $u_{\gamma j}$ governs the spin-rate; $u_{\alpha\beta j}$ is an incremental factor regulating the rotor inclination about the *X* and *Y* axes; and sat[•] indicates saturation.

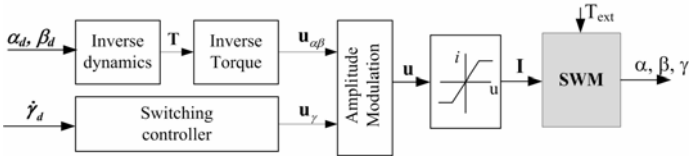

Fig. 3 OL controller of SWM

Switching (spin motion) Controller

To facilitate the design of a switching controller, we define following parameters:

Angle of plane symmetry: $\psi_{sym} = LCM(\delta_r, \delta_s) \le 180°$

Minimum step size: $\psi_{\min} = GCD(\delta_r, \delta_s)$

where *LCM* and *GCD* are the least common multiplier and greatest common divisor of their arguments.

Due to symmetry, the EM pole-pairs can be grouped into $n_{sym} = \mathrm{int}\left(360°/\psi_{sym}\right)$ phases, and only m_s / n_{sym} input currents need to be calculated. At each of the switching steps, n_{sym} PM pole-pairs align with the EM pole-pairs when projected on the *XY*-plane.

For a given $\psi_{\min}$, $n_{\max}$ levels of electronic "gear" transmission can be designed, where

$$n_{\max} = \mathrm{int}\left(\delta_r / \psi_{\min}\right).$$

The $n_{\max}$ speed levels are based on different step sizes which are an integer factor of ψ_{min}:

$$\psi = n\psi_{\min} \quad \text{where } n = 1, 2, \ldots, n_{\max}$$

For the pole-pairs defined by (1) and (2), the switching sequences with the minimum step size $\psi = \psi_{\min}$ have the form given in Table 1, where all the rows repeat after

every $S_N = 2m_s / n_{sym}$. By deduction, other different switching sequences with a step size $n\psi_{\min}$ can be made up from the sequence number S_N defined as follows:

$$S_N = nj - (n-1), \quad \text{where } j = 1, \ldots, m_s.$$

If $S_N > m_s$, $S_N = S_N - m_s$. The S_N row in Table 1 specifies the polarities of the EM's for that sequence (or time step).

Table 1 Minimum-step switching

S_N	EM pole-pairs				
	1	**2**	**3**	…	m_s / n_{sym}
1	N	S	N	⋮	N
2	N	S	N		S
⋮	N	S	N		S
$m_s / n_{sym} - 1$	N	S	S		S
m_s / n_{sym}	N	N	S		S
$m_s / n_{sym} + 1$	S	N	S		S
$m_s / n_{sym} + 2$	S	N	S		N
⋮	S	N	S		N
$2m_s / n_{sym} - 1$	S	N	N		N
$2m_s / n_{sym}$	S	S	N		N

From Table 1, the input regulating the spin takes the form:

$$u_{\gamma j} = (-1)^j \left| u_{mj} \right| \operatorname{sgn}\left[\sin(\omega_s t + \theta_j) \right] \tag{11}$$

$\omega_s = n\pi / \left(n_{\max} \Delta t_s \right)$ and $\theta_j = -\pi(n-1)/n_{\max} - jn\psi_{\min} - \theta_o$

where j = 1, 2, …, m_s ; n=1, 2, ..., n_{max}; Δt_s=update sampling rate; $0 < \theta_o < \psi_{\min}$; $\operatorname{sgn}(x) = 1, -1$ corresponding to $x \geq 0$ and $x < 0$ respectively; and ω_s is the switching frequency of the square wave. The steady-state spin-rate $\dot{\gamma}_{ss}$ is linearly proportional to ω_s and ψ while the choice of the current magnitude $\left| u_{mj} \right|$ depends on the rotor dynamics.

Inclination controller

As illustrated in Fig, 1, the rotor which is structurally symmetric and operated on the push-pull principle is open-loop stable. The rotor tends to be at the local minimum field energy states; these are local stable equilibrium positions to which the rotor would move from any perturbed position within the local boundary through the *shortest* path during the transient. The inclination control is designed about the local equilibrium (α=β=γ=*0°*). Given the desired orientation [α_d β_d], the required torque at this state is computed at γ=0 from (12a):

$$\left[\tilde{\mathbf{T}}(\boldsymbol{\alpha}, \boldsymbol{\beta}) \right] \mathbf{u}_{\boldsymbol{\alpha\beta}} = \mathbf{T}_{\mathbf{d}} \tag{12a}$$

The current to generate this torque is given by the inverse (torque) model in (12b):

$$\mathbf{u}_{\boldsymbol{\alpha\beta}} = \left[\tilde{\mathbf{T}} \right]^{\mathbf{T}} \left(\left[\tilde{\mathbf{T}} \right] \left[\tilde{\mathbf{T}} \right]^{\mathbf{T}} \right)^{-1} \mathbf{T}_d \tag{12b}$$

Once the inclination and spin currents are computed from (11) and (12) respectively, the total current inputs can be determined from (10).

In order to express the inclination control law in closed-form, we describe the inclination of a continuously spinning rotor using the ZYZ Euler angles ($\bar{\alpha}, \bar{\beta}, \gamma$). In this representation, $\bar{\alpha}$ is the rotation of the rotor shaft (or *z* axis) about the Z axis; $\bar{\beta}$ is the angle of inclination between the rotor shaft and the Z axis, and γ is the spin of the rotor shaft about its own *z* axis. Thus, for real-time computation of the coordinate transformation, we define $[\bar{\alpha}\ \bar{\beta}\ \gamma]$ in (13):

$$\bar{\beta} = \cot^{-1}\left(-\sin\beta \cot\alpha \right) \tag{13a}$$

and

$$\bar{\alpha} = \sin^{-1}\left(-\sin\alpha / \sin\bar{\beta} \right) \tag{13b}$$

The inclination controller is designed as follows:

1. The magnitude of the spin current in (11) is normalized to unity, $|u_{mj}|$=1, which maintains the spinning rotor atα=β=0. The required current vector to incline the rotor at other angle is given by (12).
2. We decouple the $\bar{\alpha}$ and $\bar{\beta}$ motion control by defining two Fourier series functions $f_{j1}(\bar{\alpha})$ and $f_{j2}(\bar{\beta})$ in (14):

$$\hat{u}_{\alpha\beta,j} = f_{j1}(\bar{\alpha}) f_{j2}(\bar{\beta}) \tag{14}$$

3. The coefficients of the two Fourier series are found by minimizing the following square-error function:

$$E_j = \left(u_{\alpha\beta,j} - \hat{u}_{\alpha\beta,j} \right)^2 \tag{14a}$$

where

$$f_{j1}(\alpha) = \sum_{i=1}^{2} \left[a_{ji} \cos(i\bar{\alpha}) + b_{ji} \sin(i\bar{\alpha}) \right] \tag{14b}$$

and

$$f_{j2}(\beta) = c_{jo} + \sum_{i=1}^{3} \left[d_{ji} \cos(i\bar{\beta}) + e_{ji} \sin(i\bar{\beta}) \right] \tag{14c}$$

The ZYZ Euler angle representation has a singularity at $\bar{\alpha} = \bar{\beta} = 0$ and is used only to obtain (14) in closed form for inclination control.

B. PD controller

PD controllers have been widely used to eliminate the effect of uncertainty and track the desired command for the control of electromagnetic actuators in a number of robotic areas. Figure 4 shows the classical PD controller with the nonlinear dynamics of the SWM.

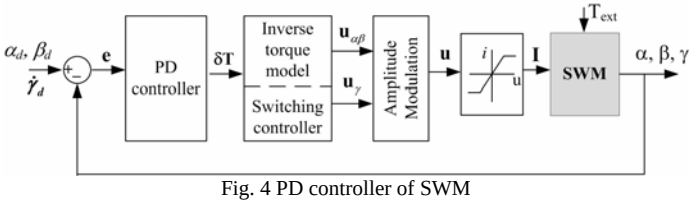

Fig. 4 PD controller of SWM

The desired torque for the PD controller is given in terms of the position tracking error as follows:

$$\mathbf{T} = [\mathbf{K_p}]\tilde{\mathbf{x}}_1(t) + [\mathbf{K_d}]\tilde{\mathbf{x}}_2(t) \tag{15}$$

where $\tilde{\mathbf{x}}_1(t) = \mathbf{q_{1d}} - \mathbf{q}_1(t)$; and $\tilde{\mathbf{x}}_2(t) = \mathbf{q_{2d}} - \mathbf{q}_2(t)$. In (15), the matrixes **[$\mathbf{K_p}$]** and **[$\mathbf{K_d}$]** are positive definite. Once the desired torque is calculated, the actual current input vector is computed from the inverse torque model (12) for the control of inclination along with (11) for the spin rate control.

Stability of PD controller

The stability of the PD controller is analyzed using the Lyapunov candidate function [9] given in (16):

$$V = \frac{1}{2}\left(\tilde{\mathbf{x}}_2^{\mathrm{T}}[\mathbf{M}]\tilde{\mathbf{x}}_2 + \tilde{\mathbf{x}}_1^{\mathrm{T}}[\mathbf{K_p}]\tilde{\mathbf{x}}_1 \right) \tag{16}$$

The time derivative of the Lyapunov function is

$$\dot{V} = \frac{1}{2}\frac{d}{dt}\left(\tilde{\mathbf{x}}_2^{\mathrm{T}}[\mathbf{M}]\tilde{\mathbf{x}}_2 + \tilde{\mathbf{x}}_1^{\mathrm{T}}[\mathbf{K_p}]\tilde{\mathbf{x}}_1\right) = -\tilde{\mathbf{x}}_2^{\mathrm{T}}\left(\mathbf{T} - [\mathbf{K_p}]\tilde{\mathbf{x}}_1\right) \qquad (16a)$$

which can be shown to be

$$\dot{V} = -\tilde{\mathbf{x}}_2^{\mathrm{T}}[\mathbf{K_d}]\tilde{\mathbf{x}}_2^{\mathrm{T}} \le 0 \qquad (16b)$$

Along with (15), (16b) implies that the Lyapunov function is only zero at $\tilde{\mathbf{x}}_2 = 0$. Therefore, the SWM with the PD controller is stable and converge to the desired state.

C. High gain observer with linear approximation

The interest to design a compact actuator with minimum hardware, an observer to estimate unmeasured outputs for a practical control design has been developed as shown in Fig. 5. The observer has been based on a linear approximation around the desired (final) states for the nonlinear dynamics (9). With the assumption that the rotor orientation can be measured by an assembly of Hall Effect sensors [10], the forward torque model (6) can be computed in real-time.

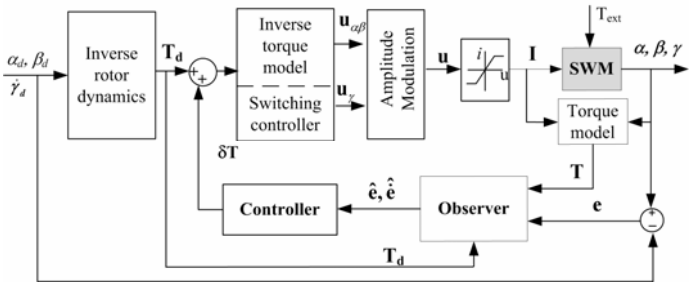

Fig. 5 High gain observer with linear approximation for error dynamics

The linear error dynamics is given in (17):

$$\begin{aligned} \dot{\tilde{\mathbf{x}}} &= [\mathbf{A}]\tilde{\mathbf{x}} + [\mathbf{B}]\mathbf{Q} \\ \mathbf{z} &= [\mathbf{C}]\tilde{\mathbf{x}} \end{aligned} \qquad (17)$$

where $[\mathbf{B}] = \left[\mathbf{0}_{3\times 3} \quad \mathbf{I}_{3\times 3}\right]^{\mathrm{T}}$ and $[\mathbf{C}] = \left[\mathbf{I}_{3\times 3} \ \mathbf{0}_{3\times 3}\right]$. To provide an estimate on the unmeasured error signals (angular velocities) around the desired state, a linear high-gain (full state) observer for the tracking error dynamics is designed. In terms of estimated state $\hat{\mathbf{x}} = \mathbf{q}_d - \hat{\mathbf{q}}$,

$$\begin{aligned} \dot{\hat{\mathbf{x}}} &= [\mathbf{A}]\hat{\mathbf{x}} + [\mathbf{B}]\mathbf{Q} + [\mathbf{H}](\mathbf{z} - \hat{\mathbf{z}}) \\ \hat{\mathbf{z}} &= [\mathbf{C}]\hat{\mathbf{x}} \end{aligned} \qquad (18)$$

The dynamics of the estimated error $\mathbf{e} = \tilde{\mathbf{x}} - \hat{\mathbf{x}}$ is then given by

$$\dot{\mathbf{e}} = \left([\mathbf{A}] - [\mathbf{H}][\mathbf{C}]\right)\mathbf{e} = [\Lambda]\mathbf{e} \qquad (19)$$

In (18) and (19), $[\mathbf{H}] = \text{Block Diag}\left[\mathbf{H}_1 \ \mathbf{H}_2\right]^{\mathrm{T}}$ where $\left[\mathbf{H}_j\right] = \text{Diag}\left[\alpha_j^1/\varepsilon^j \quad \alpha_j^2/\varepsilon^j \quad \alpha_j^3/\varepsilon^j\right]$; ε^j (j=1,2) is a positive constant to be specified; and the positive constants α_j^i are chosen such that the roots of (20) satisfy time response specifications in the left-half plane of the complex domain. It guarantees asymptotic error convergence $\lim_{t\to\infty}\mathbf{e}(t) = 0$. This indicates the stability of the observer dynamics.

$$\det\left|s\mathbf{I} - [\Lambda]\right| = 0 \qquad (20)$$

The separation principle allows us to design the controller and observer separately to guarantee the stability of the overall system. The stability of the PD controller has been shown in (16), and can be extended to include the high gain observer.

SIMULATION RESULTS

The effectiveness of the controllers for the SWM (Fig. 1) is illustrated by simulation. The parameters used in the simulation are detailed in Tables 2 and 3.

Table 2 Stator and rotor pole pair

Stator EM pole	OD = 0.75 in, 1050 turns
Coil wire and resistance	29 AWG, 6.46 Ohms
Current (2 EM's in series)	4 Amperes
Rotor radius	76.2 mm (3 inches)
Cylindrical PM	OD=L=12.5mm (0.5in)
Air-gap between EM & PM	0.762mm (0.03in)

Table 3 Values used in the setup

Rotor radius		76.2 mm (3 inches)
	Offset of mass centre	$\vec{r} = 0$
	M. of Inertia, (kg-m^2)	I_a = 6.0576e-005; I_t =3.8628e-005
	Frictional coefficient $\mathbf{C}_f$	0.3 Nm•sec
Stator EM's		20 (2 layers of 10)
	Magnetization	$\phi_s = 26°$; $\delta_s = 36°$
	Current limit	u_{sat} = 1 Ampere
Rotor PM's		16 (2 layers of 8)
	Magnetization	$\phi_r = 20°$; $\delta_r = 45°$

R=d=6.35mm, g=0.5mm, and $\mu_0 M_0$=1.35Tesla

Spin motion

For the SWM (Fig.1), $\psi_{sym} = 180°$ implies that the 10 (pole-pairs of) EM's can be divided into $n_{sym} = 2$ phases; the 6th to 10th EM's have the same current profiles as 1st to 5th EM's respectively. Additionally, the minimum step size of $\psi_{\min} = 9°$ suggests that $n_{\max} = 5$ different spin-speed levels can be designed for the OL control. The plan view showing the EM layout and he switching sequences for five different spin-speed levels ($n = 1, 2...5$) are given in Table 4, upon which the switching current can be intuitively derived as follows:

1. From the current polarity in Table 1, the switching current vector $\mathbf{u}_\gamma$ is obtained and shown in Fig. 6, where the horizontal axis indicates S_N (which is also the time step).
2. For a particular speed level n, the switching current has a period T which depends on the number of sequences S_N and is given (in terms of sampling interval Δt_s) in Table 4.
3. Each time step the rotor spins $\psi = n\psi_{\min}$ degrees and the rotor requires $360/\psi$ steps to complete one revolution. Thus, the spin rate (in rpm) directly depends on n and Δt_s. Table 5 shows an example for Δt_s=1 ms.

The switching current can also be expressed mathematically (11), where ω_s and θ_j are given in Table 5 (θ_o=5°, Δt_s=1 ms).

Table 4: Switching controller for $n = 1, 2...5$ spin-speed levels

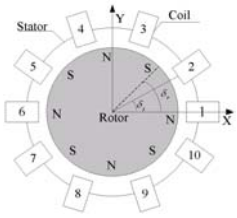

Plan view of coil layout

n	ψ	S_N	Period, T
1	9°	*1, 2, 3, 4, 5, 6, 7, 8, 9, 10*	90°, 10Δt_s
2	18°	*1, 3, 5, 7, 9*	90°, 5Δt_s
3	27°	*1, 4, 7, 10, 3, 6, 9, 2, 5, 8*	270°,10Δt_s
4	36°	*1, 5, 9, 3, 7*	180°, 5Δt_s
5	45°	*1, 6*	90°, 2Δt_s

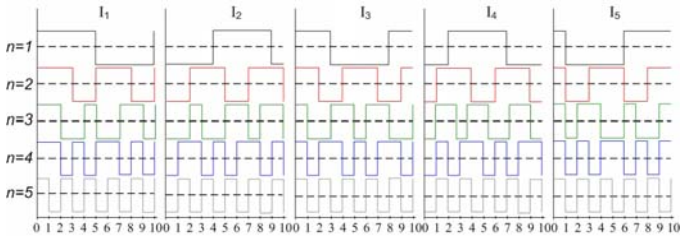

Fig. 6 Timing diagram for five different spin-speed levels

Table 5: Parameters of switching controller

n	θ_j	ω_s (rad/s)	T(ms)	$\dot{\gamma}_{ss}$ rpm
1	*-0.1571j-0.0873*	628	10	1500
2	*-0.3142j*-0.7156	1,257	5	3000
3	*-0.4713j-1.3439*	1,885	10	4500
4	*-0.6284j-1.9723*	2,513	5	6000
5	*-0.7855j-2.6006*	3,142	2	7500

θ_o=5 °, Δt_s=1ms

OL Inclination

The OL inclination controller (14) has been optimized minimizing (14a) using the MATLAB Optimization toolbox; the computed unknown parameters in (14b, c) are detailed in Tables 6 and 7 for $\bar{\alpha}$ and $\bar{\beta}$ respectively.

The computed currents of the OL inclination controller are plotted in Figs. 7(a)-(e) showing the current profiles of the 1st to 5th EM's. Figure 7(f) shows the current components at $\bar{\beta} = \phi_s - \phi_r = 6^o$ (Fig. 1b) when the 1st pair of EM aligns with the PM. Due to the symmetrical structure designed to operate on the push-pull principle, it can be easily shown using (12b) that the currents to 6th to 10th EM's have the equal magnitude but opposite direction to that to 1st to 5th EM's. Similar arguments can be made for the pairs j=2,5 and j=3,4 as shown in Fig. 7(f).

Table 6 Fourier series constant for the inclination $\bar{\alpha}$ current vector

J	1	2	3
a_{i1}	-134.896	-144.083	-101.69
a_{i2}	134.89	144.074	101.682
b_{i1}	6374.87	5162.52	3843.15
b_{i2}	-3185.02	-2579.32	-1919.34

Due to the symmetry about $\bar{\alpha}$, $u_{\alpha\beta,5}=u_{\alpha\beta,2}$, $u_{\alpha\beta,4}=u_{\alpha\beta,3}$.

Table 7 Fourier series constant for the inclination $\bar{\beta}$ current vector

J	1	2	3	4	5
c_{io}	.035466	-0.091224	-0.003365	-0.003365	-0.091224
d_{i1}	.02134	-0.130895	0.013119	-0.036560	-0.12672
d_{i2}	-0.09967	0.040402	0.005075	-0.003483	0.055141
d_{i3}	-0.01214	-0.054836	0.003483	-0.005075	-0.048777
e_{i1}	-0.47508	0.126491	0.03656	0.013119	-0.142679
e_{i2}	-0.02024	0.165207	-0.032600	0.032600	-0.158953
e_{i3}	.118731	0.032188	-0.023501	0.023501	-0.037096

Feedback Control

The controller gain matrices for the PD controller are set to $[K_p]$=23I $[K_d]$=I, which minimize the current input saturation. For the high-gain observer, the parameters $\varepsilon^1=\varepsilon^2$=0.01 and α^i_j = –5 (i=1,2 and j=1,2,3) are used. The eigenvalues are compared as follows:

PD: -0.98±31.52j; -0.02±0.73j; -0.50±4.77j

Observer (×100): -1.34±j0.49; -3.66±j0.18; -3.62; -1.38

Thus, the observer dynamics is faster than that of the controller.

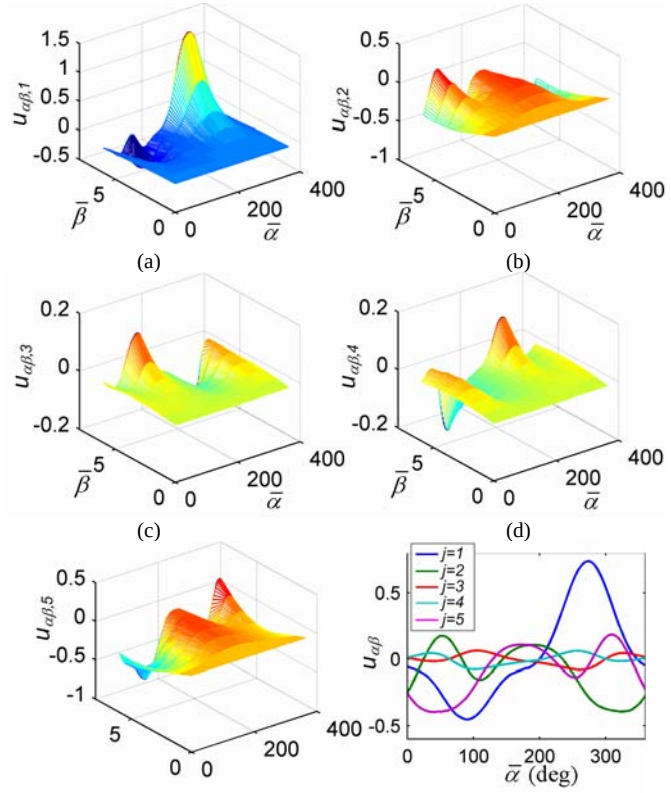

Fig. 7 Inclination current inputs

Figure 8(a) shows the rotor trajectory from an arbitrary initial position (α=β=0, γ=30°) to the desired position (α=5°, β=γ=0°). The corresponding torque is given in Fig. 8(b). This initializes the rotor which is then commanded to spin at the specified inclination. Figure 9 shows the simulation results at α=5° (0.0873 radians), β=0° and $\dot{\gamma} = 19.6$ rad/sec (187.5 rpm) with a constant external torque $\mathbf{T_{ext}} = [0.05\ 0\ 0]^T$ Nm. The simulation results of the model-based OL controller and the PD controller with/without the high-gain observer are compared. The maximum steady state error of the controllers is compared in Table 8. As expected, the OL alone cannot compensate any unknown torque. The addition of a feedback loop successfully drives the rotor to the desired orientation, and attenuates oscillations. The error dynamics with a high gain observer converge to zero faster than the classical PD controller.

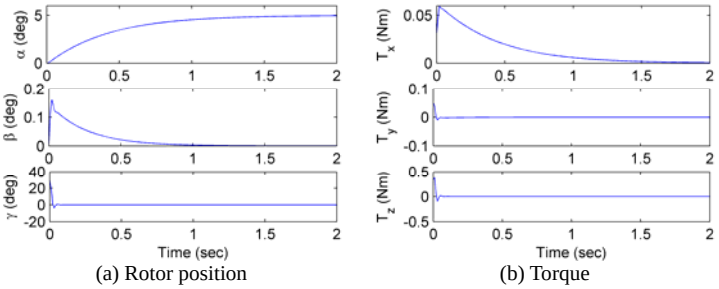

(a) Rotor position (b) Torque

Fig. 8 Initialization to the desired position (α=5°,β=γ=0°)

CONCLUSIONS

We presented three controllers for a multi-DOF spherical actuator (SWM). The first is a model-based open-loop (OL)

controller which serves as an essential basis for feedback control system designs. The OL control presented here offers an effective method to decouple the control of the spin rate from that of the inclination and thus allow the OL controller to consist of two independent parts; a switching (spin-rate) controller based on the principle of a stepper, and an inclination controller based on the inverse torque model. The OL controller shows the feasibility of operation without any disturbance. We further extend the design to allow feedback controller to be implemented. In this study, we simulate the closed loop controller for output tracking and disturbance rejection.

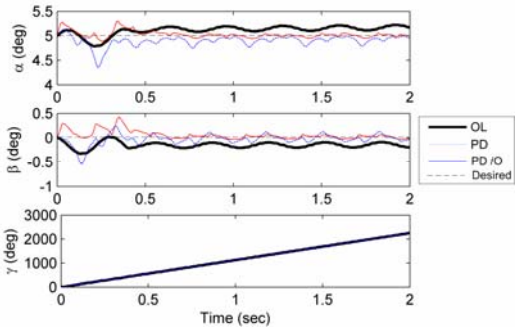

(a) Output Tracking for desired Euler angles (α=5°,β=0)

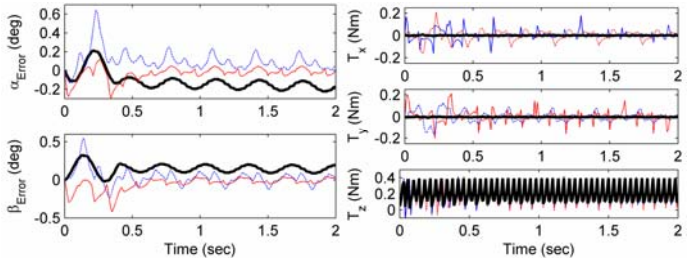

(b) Error of inclination (c)Torque

Fig. 9 Simulation comparisons

Table8 Maximum steady state Error ($|E_{ss}|$)

Max($\|E_{ss}\|$) (deg)	OL	PD	PD with Observer
α	0.24	0.20	0.05
β	0.19	0.07	0.04

REFERENCES

[1] Lee, K.-M. and C. Kwan, "Design concept development of a spherical stepper for robotic applications", *IEEE Trans. on Robotics and Automation*, 1991. **7**(1).

[2] Hollis, R. L., S. E. Salcudean, and A. P. Allan, "A six-degree-of-freedom magnetically levitated variable compliance fine-motion wrist: design, modeling, and control", *IEEE Trans. Robot. Automat.*, 1991. p. 320-332.

[3] Chablat, D. and Wenger, P, "Architecture optimization of a 3-DOF translational parallel mechanism for machining applications, the orthoglide", *IEEE Trans. Robot. Automat.*, 2003., pp. 403-410.

[4] Ueda, R., H. Takata, S. Nakagaki, and S. Takata, "On the estimation of transient state of power system by discrete nonlinear observer", IEEE Trans. on Power Apparatus and Systems, 1975. PAS-94(6) p. 2135-2140.

[5] Jones, L. A. and J. H. Lang, "State observer for the permanent-magnet synchronous motor", IEEE Trans. on Industrial Electronics, 1989. 36(3) p. 374-382.

[6] Dabroom, A. M. and H. K. Khalil, "Output feedback sampled-data control of nonlinear systems using high-gain observers", IEEE Trans. on Automatic Control, 2001. 46(11) p. 1712-1725.

[7] Zhu, G., A. Kaddouri, L. A. Dessaint, and O. Akhrif, "A nonlinear state observer for the sensorless control of a permanent-magnet AC machine", IEEE Trans. on Industrial Electronics, 2001. 48(6) p. 1098-1108.

[8] Lee, K.-M. and H. Son. "Torque model for design and control of a spherical wheel motor", IEEE/ASME AIM2005 Proc., pp. 335-340.

[9] Lee, K.-M. R. A. Sosseh and Z. Wei, "Effects of the Torque Model on the Control of a VR Spherical Motor," *IFAC Journal of Control Engineering Practice*, Vol. 12, pp 1437-1449, 2004.

[10] H. Son and K.-M. Lee "Distributed multi-pole model for motion simulation of PM-base spherical motor," IEEE/ASME AIM2007.

[11] Lee, K.-M. and H. Son, "Equivalent Voice-coil Models for Real-time Computation in Electromagnetic Actuation and Sensor Applications," IEEE/ASME AIM2007.

NOMENCLATURE

Capitalized symbols

[A]	Linearized system matrix
[B]	Input matrix
[C]	Output matrix
C	Coriolis matrix
$\mathbf{C_f}$	Friction matrix
E_j	Error of j^{th} current
F	*x,y,z* component forces
T	*x,y,z* component torque
$\mathbf{K_p}$	Proportional gain matrix
$\mathbf{K_d}$	Derivative gain matrix
I	Current
I_a,	Moment of inertia along z
I_t	Moment of inertia along x,y
J	Current density
L	Transformation matrix
[M]	Mass matrix
M_o	Magnetization
S_N	Sequence Number
T	Period time
$\mathbf{T_{ext}}$	External torque vector
S_x	sin (x)
C_x	cos(x)
Q	Generalized torques
V	Lyapunov function

Lowercase symbols

i	The number of PM
j	The number of EM
e	Estimation error
m_r	Number of PM
m_s	Number of EM
n	Sequence number
q	Generalized coordinates
u_γ	Control inputs of spin
$u_{\alpha\beta}$	Control inputs if inclination
u_s	Control inputs
$\hat{u}$	Estimation of current function
$\tilde{\mathbf{x}}$	Error state vector
$\tilde{\mathbf{z}}$	Estimation Error state vector

Greek letter symbols

α, β, γ	ZYZ Euler angles
$\bar{\alpha},\bar{\beta},\bar{\gamma}$	XYZ Euler angles
ϕ_r,	Separation angle between PM and XY plane
ϕ_s	Separation angle between EM XY plane
ε	Positive constant for observer
δ_r, δ_s	Separation angle of PM ,EM
Ψ_{min}	Angle of minimum step
Ψ_{sym}	Angle of plane symmetry
μ_o	free space permeability

ACKNOWLEDGMENTS

This project has been funded jointly by the U .S. Poultry and Eggs Association and the Georgia Agricultural Technology Research Program.